PAPER

Check for updates

Citrate-gel preparation and ammonia synthesis activity of compounds in the quaternary (Ni, M)$_2$Mo$_3$N (M = Cu or Fe) systems†

Samia Al Sobhi,[a] Justin S. J. Hargreaves,*[b] Andrew L. Hector [ID] *[a] and Said Laassiri[b]

Single phase solid solutions based on copper and iron substitution into the nickel sites of Ni$_2$Mo$_3$N are produced using a citrate gel approach followed by ammonolysis. These metal nitrides show good ammonia synthesis activity at 500 °C and ambient pressure. The activity fell with copper content and increased with iron content, although these changes appear to be related to the surface areas of the catalysts. The oxide intermediates from the citrate gel process cleanly converted to the metal nitride under the ammonia synthesis gas stream (75% H$_2$, 25% N$_2$) providing more active catalysts than those pre-nitrided by ammonolysis.

Introduction

The Haber–Bosch process directly sustains a major fraction of the world's population by providing a route from N$_2$ to fertilisers, and demand could rise if ammonia is employed significantly as a carbon-free fuel. However, Haber–Bosch consumes 1–2% of the world's energy supply and results in significant carbon emissions in necessarily centralised (so poorly suited to renewable energy use) environments.[1] Hence the search for catalysts that can operate effectively under lower pressure and temperature environments, or with less pure feedstocks, continues to be important even after many decades of operation of the Haber–Bosch process.

Interest in metal nitrides as heterogeneous catalysts has focussed on hydrotreating reactions such as heteroatom removal and hydrogenations, often using high surface area molybdenum nitride derived from temperature programmed ammonolysis reactions of oxides or other molybdenum compounds.[2–4] However, the high ammonia synthesis activity of some ternary molybdenum nitrides has also attracted significant work on these compounds. Notably Co$_3$Mo$_3$N can outperform commercial iron-based Haber–Bosch catalysts,[5,6] with its high activity linked to the possible operation of a Mars–van Krevelen type process.[7,8] It is also an active electrocatalyst for ammonia synthesis.[9] We previously reported quaternary compounds in the (Ni,Co)$_2$Mo$_3$N system with good activity for ammonia synthesis.[10,11] The principle of electronic tuning through substitution of one of the atoms is used extensively in catalysis, and could be useful in optimising activity of ternary nitrides.

The filled β-Mn structure adopted by Ni$_2$Mo$_3$N contains distorted, corner sharing NMo$_6$ octahedra interpenetrated with a (10,3)-network of nickel atoms (Fig. 1).[12,13] Complex metal
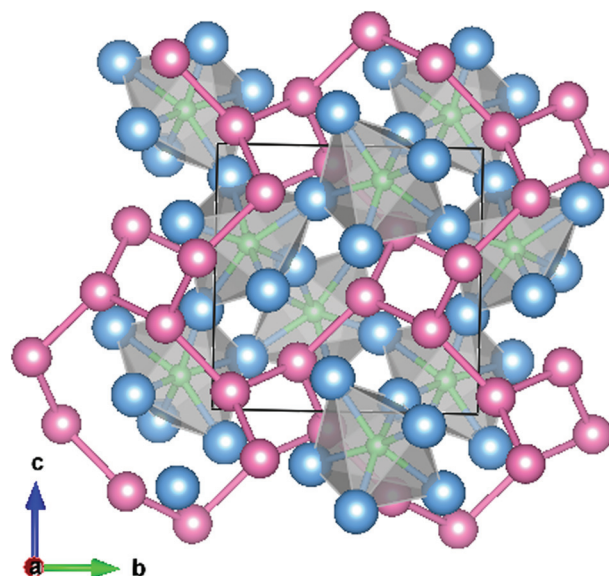

Fig. 1 Unit cell of Ni$_2$Mo$_3$N viewed along [100] showing the corner linked NMo$_6$ octahedra and the interpenetrating (10,3)-network of nickel atoms. Nickel atoms are shaded pink, molybdenum blue and nitrogen green. Diagram prepared using Vesta and structure data from Prior and Battle.[13]

[a]School of Chemistry, University of Southampton, Highfield, Southampton SO17 1BJ, UK. E-mail: A.L.Hector@soton.ac.uk

[b]WestCHEM, School of Chemistry, University of Glasgow, Joseph Black Building, Glasgow G12 8QQ, UK. E-mail: Justin.Hargreaves@glasgow.ac.uk

†Electronic supplementary information (ESI) available. See DOI: 10.1039/c9dt03673c

nitrides are often made *via* the high temperature ammonolysis of an oxide with the desired metal atom ratio, for example $CoMoO_4$ produces Co_3Mo_3N.[6] Attempts at this approach in the Ni_2Mo_3N system have led to metal contamination and a much reduced ammonia synthesis activity.[10,14] The use of a citrate gel to produce an intimate mix of metal oxides that forms the filled β-Mn phase on ammonolysis was successful in producing active Ni_2Mo_3N and $(Ni,Co)_2Mo_3N$ catalysts.[10] Copper substitution of the nickel sites in Ni_2Mo_3N has not previously been reported, but the citrate gel process requires merely a water soluble copper source and was considered likely to produce phases in this space. We show herein that $(Ni,Cu)_2Mo_3N$ phases do exist up to a solubility limit, produce $(Ni,Fe)_2Mo_3N$ compositions by the same route, and determine the effect of copper and iron substitution on ammonia synthesis activity.

Experimental

Nanocrystalline samples of $Ni_{2-x}M_xMo_3N$ (M = Cu or Fe) were prepared by a citrate gel route followed by ammonolysis. Stoichiometric amounts of $(NH_4)_6Mo_7O_{24}·4H_2O$ (2 g, Sigma Aldrich, 99.9%), $Ni(NO_3)_2·6H_2O$ (Sigma Aldrich, 99.9%) and either $Cu(NO_3)_2·4H_2O$ (Sigma Aldrich, 99%) or $Fe(NO_3)_2·6H_2O$ (Sigma Aldrich, 99.95%) were dissolved in 60 cm^3 aqueous HNO_3 (2.6 mol dm^{-3}, prepared from Fisher Scientific 70% HNO_3, used for ammonium molybdate solubility). Citric acid monohydrate (7.935 g, Sigma Aldrich, ACS reagent, ≥99%) was then added to the green solution. Actual quantities are given in ESI, Table S1.† The green solution was evaporated in a sand bath at 70 °C to ~10 cm^3 of viscous green gel (ESI, Fig. S1†), then heated in an ashing furnace (60 °C min^{-1} heating rate) at 500 °C for 2 h. The resulting grey foam was ground to a powder then heated in flowing ammonia (BOC anhydrous grade, further dried with molecular sieves) at 5 °C min^{-1} to 900 °C and maintained for 12 h. Once cool, the furnace tube was flushed with N_2 for 30 min then air was allowed to diffuse in slowly to passivate sample surfaces before the black crystalline product was recovered. Samples were then handled under aerobic conditions during characterisation. *Caution: a sand bath was used because citrate gels can occasionally ignite; the unpassivated metal nitrides are highly pyrophoric.*

The powder X-ray diffraction (PXRD) patterns of the samples were collected using a Bruker D2 Phaser X-ray diffractometer with Cu-$K_α$ radiation. The Rigaku PDXL2 package and the PDF database[15] were used for pattern matching. Rietveld refinement was carried out using GSAS[16,17] and structure models from ICSD.[18] Scanning electron microscopy (SEM) was conducted using a Philips XL-30 ESEM (20 kV accelerating voltage) with a ThermoFisher Ultradry energy dispersive spectroscopy (EDS) detector and Noran System 7 data processing. Transmission electron microscopy (TEM) was performed on Hitachi H7000 with accelerating voltage of 75 kV with samples prepared by ultrasound dispersal in propan-2-ol and deposition on carbon-coated copper grids. Thermogravimetric analysis (TGA) used a Netzch TG 209 F1 Libra instrument with a

heating rate of 10 °C min^{-1} under 40 mL min^{-1} of 50% oxygen and 50% argon. The surface areas of the samples were calculated by applying the Brunauer, Emmett and Teller[19] (BET) method to nitrogen physisorption isotherms measured at 77 K using a Micromeritics Tristar II and samples previously degassed overnight at 120 °C. Combustion (CHN) analysis was outsourced to Medac Ltd.

The catalytic performance of the obtained catalysts in ammonia synthesis was evaluated by a method similar to that described previously.[20] The catalyst (0.15 g) was loaded in the centre of a 4.2 mm internal diameter silica tube as a plug held in place by a sinter, then placed in a tube furnace. 13 mL min^{-1} 75% hydrogen/25% nitrogen gas mixture (BOC, H_2 99.998%, N_2 99.995%) was passed through the tube and it was heated to 700 °C for 2 hours to activate the catalyst followed by lower temperature steps to test ammonia production. On reaching the reaction temperature, the vent gas from the reactor was bubbled through a dilute solution of sulfuric acid (0.001 mol dm^{-3}, 100 ml) at ambient temperature and the rate of ammonia production was calculated from the conductivity decrease of the sulfuric acid solution with time (Orion Star A212 Portable Conductivity Meter).[20] A linear decrease in conductivity *versus* time was observed during the measurement using H_2/N_2 as the reactant gas. Detailed calculations of ammonia production rates are given in ESI (note S1†).

Results and discussion

The advantage of citrate gel synthesis to produce solid solutions in the $(Ni,M)_2Mo_3N$ (M = Cu or Fe) system is that the 3d metals are mixed in solution, so could be well distributed in the products. A range of compositions was made starting with Ni_2Mo_3N and replacing nickel with copper or iron. Previously in the $(Ni,Co)_2Mo_3N$ system we fired samples at 700 °C and found that, in addition to the filled β-manganese type phases, they contained a trace of a rocksalt-type impurity that resembled γ-Mo_2N.[10] The filled β-manganese structure has been discussed in more detail elsewhere.[12,13] Firing Ni_2Mo_3N samples at temperatures between 600 and 1000 °C, the samples produced below 800 °C were found to contain the rocksalt-type phase (ESI, Fig. S2†), but at 900 or 1000 °C the phase pure filled β-manganese material was produced. The lattice parameters increased slightly with temperature (ESI, Fig. S3†). Hence the $(Ni,M)_2Mo_3N$ (M = Cu or Fe) used herein were produced at 900 °C.

Fig. 2 shows PXRD patterns for a series of $(Ni,Cu)_2Mo_3N$ compositions produced at 900 °C. Compositions from Ni_2Mo_3N to $Ni_{1.7}Cu_{0.3}Mo_3N$ were identified as the single phase filled β-manganese structure (space group $P4_132$). However, as the copper content was increased further, γ-Mo_2N and copper metal appeared in the patterns and grew in intensity. The lattice parameter variation obtained from Rietveld refinement of the diffraction data (ESI, Fig. S4–S12 and Table S2†) is shown in Fig. 2. The lattice parameters show a Vegard trend in the single phase compositions, suggesting a good distribution of copper in the solid solutions. The values increase with
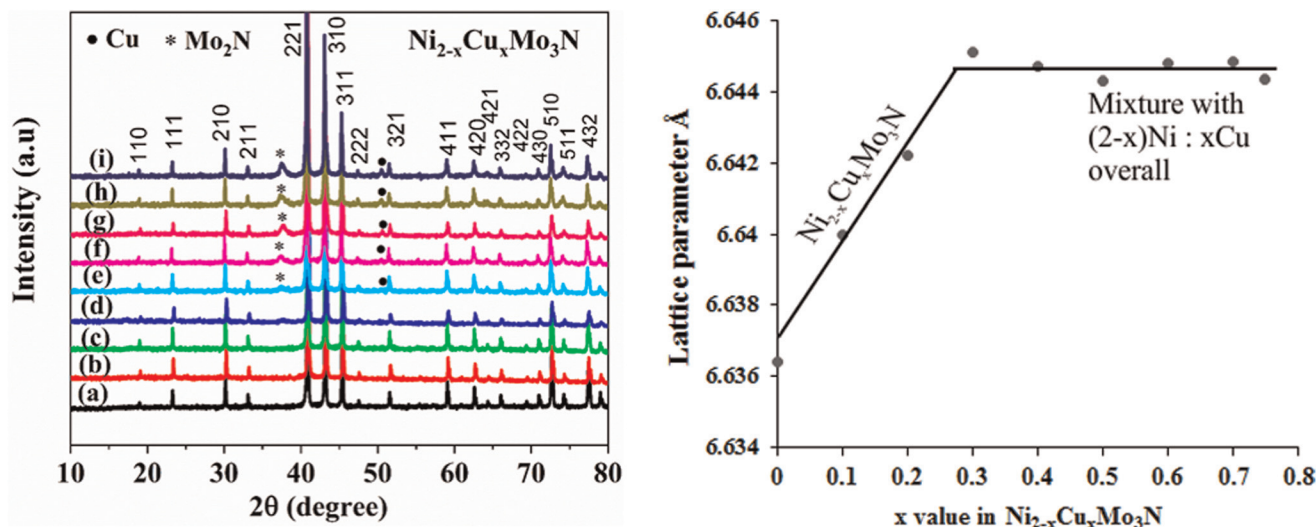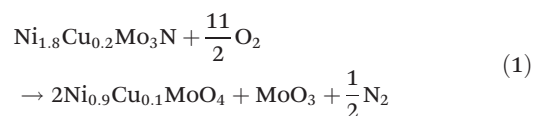
Fig. 2 Left: Powder XRD patterns for $Ni_{2-x}Cu_xMo_3N$ (overall composition x = 0 to 0.75) synthesized by firing the dry powder at 900 °C for 12 hours under NH_3 gas, where x = 0.0 (a), 0.1 (b), 0.2 (c), 0.3 (d), 0.4 (e), 0.5 (f), 0.6 (g), 0.7 (h) or 0.75 (i). Asterisks indicate the Mo_2N reflections and black circles show reflections of Cu metal. Right: The lattice parameter of the filled β-manganese phase *versus* the concentration of Cu in $Ni_{2-x}Cu_xMo_3N$, with lines added as a guide to the eye.

copper content as expected from the larger metallic radius of Cu (1.28 Å) compared with Ni (1.24 Å).[21] The lattice parameter of the filled β-manganese phase is then constant for overall compositions from $Ni_{1.7}Cu_{0.3}Mo_3N$ to $Ni_{1.25}Cu_{0.75}Mo_3N$. Hence no further copper had been introduced into the Ni_2Mo_3N structure and the limit of solubility of Cu in Ni_2Mo_3N is around the $Ni_{1.7}Cu_{0.3}Mo_3N$ composition.

EDX showed that the Ni : Mo ratio of the Ni_2Mo_3N sample to be 36.4 : 63.6 (expected 40 : 60 for Ni_2Mo_3N). As copper was substituted in, the copper contents were measured a little below the nominal compositions, but with an increasing trend (ESI, Table S3†). Note there is some overlap between the nickel and copper EDX peaks so there is a significant uncertainty in the analysis of these small amounts of copper. The composition was also tested by TGA (Fig. 3), with the samples heated in an oxygen-rich gas mixture to convert it to oxides containing Ni(II), Cu(II) and Mo(VI) (mass gain) as shown in eqn (1) (post-TGA XRD data shown in Fig. S13–S15†). The mass was unchanged up to ~330 °C, above which the oxidation of the material was observed with a resulting mass increase. This occurred in three distinct steps, with an overall mass increase of 38.30% observed by 550 °C for Ni_2Mo_3N. No further mass increases were observed above 650 °C, but mass was lost sharply above 750 °C. This can be attributed to the sublimation of MoO_3.[22] The mass gains for the Cu-doped compositions (ESI, Table S4†) were consistent with expected values. As more Cu is introduced to the lattice the oxidation temperature decreases (Fig. 3).

$$Ni_{1.8}Cu_{0.2}Mo_3N + \frac{11}{2}O_2$$

$$\rightarrow 2Ni_{0.9}Cu_{0.1}MoO_4 + MoO_3 + \frac{1}{2}N_2 \qquad (1)$$

Not only the crystalline structure and the chemical composition are important to understand the catalytic properties, the
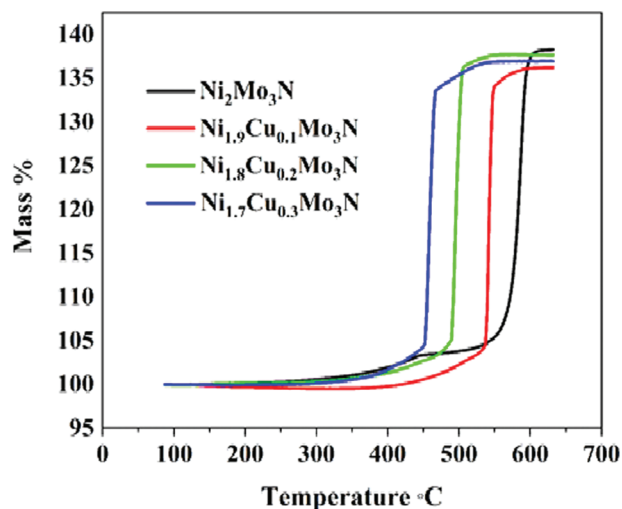

Fig. 3 TGA curves (50% O_2/50% Ar environment) showing mass gain % of the Ni_2Mo_3N, $Ni_{1.7}Cu_{0.3}Mo_3N$, $Ni_{1.8}Cu_{0.2}Mo_3N$ and $Ni_{1.9}Cu_{0.1}Mo_3N$ samples prepared at 900 °C with heating rate of 5 °C min^{-1} under ammonia.

morphology of the catalyst can also be significant. Fig. 4 shows typical images of a $Ni_{1.7}Cu_{0.3}Mo_3N$ sample obtained at 900 °C. An open structure of interconnected, rounded particles with diameters around 200 nm were found, which is in a good correlation with the average crystallite diameter of 140 nm calculated using an adaptation of the Scherrer equation incorporated into the Rietveld fitting package.[16]

The ammonia synthesis rates measured for the (Ni, Cu)$_2$Mo$_3$N samples are summarised in Table 1, alongside the BET surface areas and the nitrogen contents measured from combustion (CHN) analysis (expected wt% N is 3.3%). It is
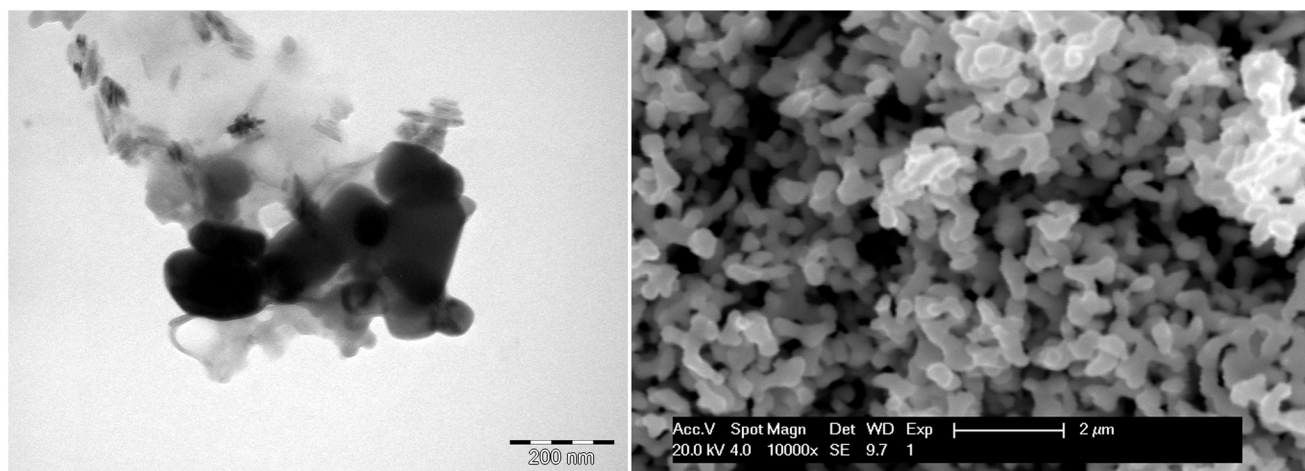
Fig. 4 TEM (left) and SEM (right) images of $Ni_{1.7}Cu_{0.3}Mo_3N$ obtained from the citrate-gel derived metal oxide precursors heated in ammonia at 900 °C for 12 hours.

Table 1 BET surface areas, elemental analysis, ammonia synthesis rate and specific activity of $(Ni,Cu)_2Mo_3N$

Catalyst	Surface area $(m^2\ g^{-1})$	Crystallite diameter (nm)	Nitrogen content[a] (wt%)		Ammonia synthesis rate at 500 °C[b] $(\mu mol\ h^{-1}\ g^{-1})$	Specific activity at 500 °C $(\mu mol\ h^{-1}\ m^{-2})$
			Pre-catalysis	Post-catalysis		
Ni_2Mo_3N	2.2	113(2)	3.4	3.3	272(5)	124(2)
$Ni_{1.9}Cu_{0.1}Mo_3N$	2.1	119(3)	3.6	3.4	252(2)	120(1)
$Ni_{1.8}Cu_{0.2}Mo_3N$	1.8	126(5)	3.6	3.4	231(2)	128(1)
$Ni_{1.7}Cu_{0.3}Mo_3N$	1.6	142(11)	3.6	3.4	179(6)	112(4)

[a] Calculated values are 3.3%. [b] Conductivity profiles used to calculate these rates are shown in ESI (Fig. S16†).

Fig. 5 Left: Magnified PXRD patterns of $Ni_{2-x}Fe_xMo_3N$, with asterisks indicating Mo metal reflections and diamonds the reflection of Fe_2N. A wider 2θ range is shown in ESI (Fig. S19†). Right: Lattice parameters obtained by Rietveld refinement (ESI, Fig. S20–S27 and Table S7†) *versus* the concentration of Fe in the $(Ni,Fe)_2Mo_3N$ systems.

noteworthy that the rate of ammonia synthesis reduces systematically with copper doping. The need to produce these samples at a relatively high temperature of 900 °C has resulted in quite low surface areas, and the surface area is reducing with increasing copper content. This can be attributed partly to crystallite growth and partly to agglomeration, both occur-

Table 2 BET surface areas, elemental analysis, ammonia synthesis rate and specific activity of $(Ni,Fe)_2Mo_3N$

Catalyst	Surface area $(m^2\ g^{-1})$	Crystallite diameter (nm)	Nitrogen content[a] (wt%)		Ammonia synthesis rate at 500 °C[b] $(\mu mol\ h^{-1}\ g^{-1})$	Specific activity at 500 °C $(\mu mol\ h^{-1}\ m^{-2})$
			Pre-catalysis	Post-catalysis		
Ni_2Mo_3N	2.2	113(2)	3.4	3.3	272(5)	124(2)
$Ni_{1.8}Fe_{0.2}Mo_3N$	2.4	142(12)	3.5	3.4	311(2)	130(1)
$Ni_{1.5}Fe_{0.5}Mo_3N$	2.5	119(10)	3.5	3.4	322(2)	129(1)
$Ni_{1.2}Fe_{0.8}Mo_3N$	2.7	114(1)	3.6	3.4	337(4)	125(1)
$Ni_{1.1}Fe_{0.9}Mo_3N$	2.8	103(2)	3.6	3.2	354(4)	126(2)

[a] Calculated values are 3.3–3.4%. [b] Conductivity profiles used to calculate these rates are shown in ESI (Fig. S28†).
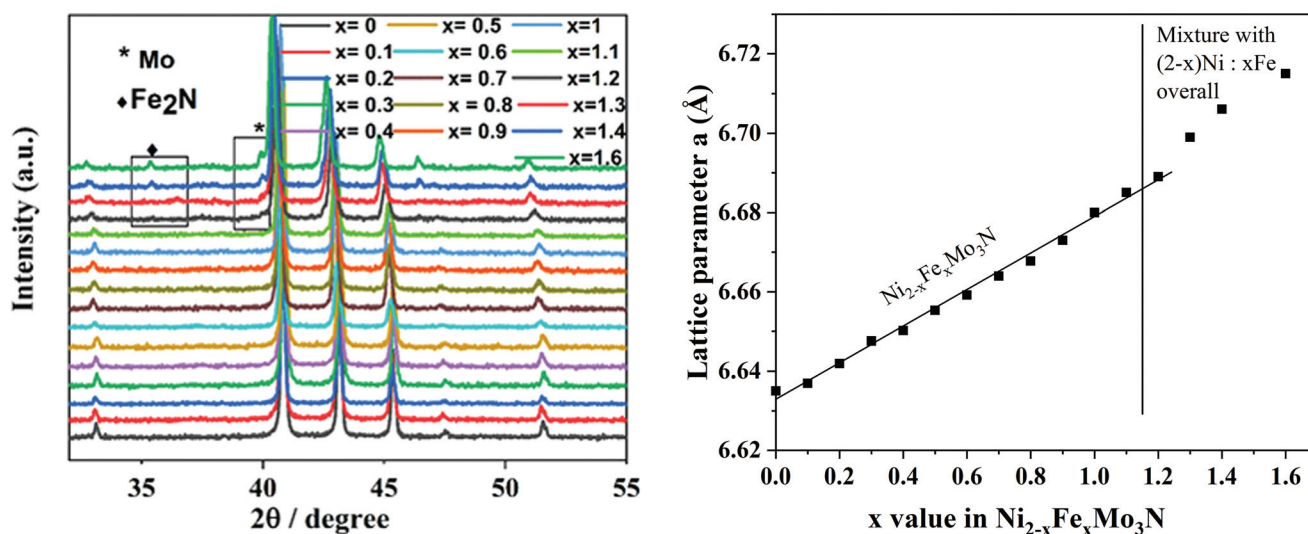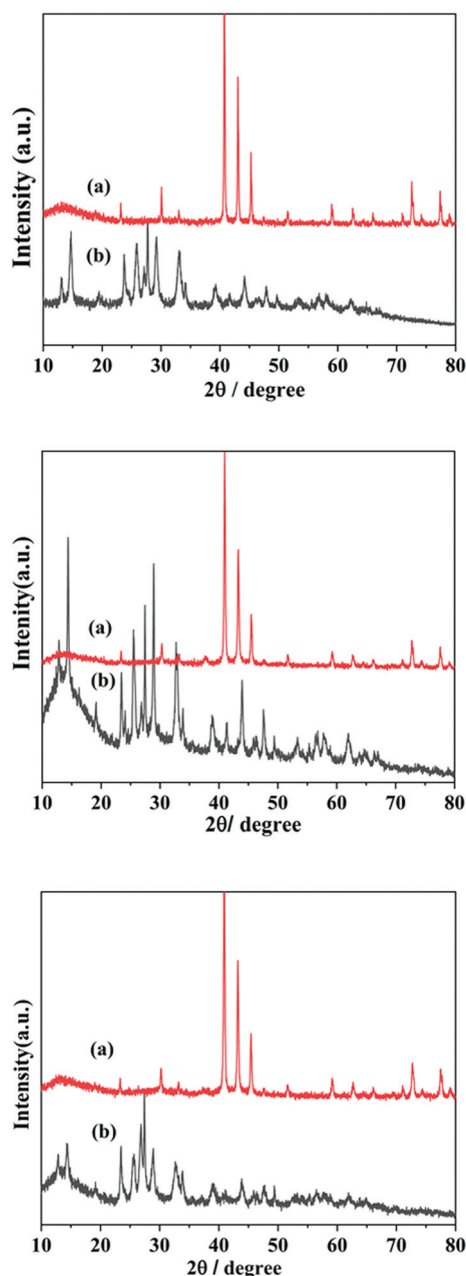
Fig. 6 PXRD patterns of catalysts after (a) and before (b) use in ammonia synthesis. The precursor compositions were $Ni_2Mo_3O_x$ (top), $Ni_{1.7}Cu_{0.3}Mo_3O_x$ (centre) and $Ni_{1.2}Fe_{0.8}Mo_3O_x$ (bottom).

ring through sintering at this high reaction temperature, but the surface areas are fairly typical for this type of material.[23] However, the surface area of Mo based nitride materials can be strongly influenced by synthesis factors such as NH_3 flow rates and temperature ramp rates,[24–27] and achieving higher surface areas should be a future priority.

Substituting iron into the Ni_2Mo_3N, the synthesis proceeded in the same way as for copper except that a brown colour developed as the sol was concentrated (ESI, Fig. S1†). After firing in ammonia at 900 °C the PXRD showed phase pure filled β-manganese-structured samples with iron contents up to $NiFeMo_3N$ (Fig. 5). An increasing linear trend in lattice parameter with iron content indicates the formation of well distributed solid solutions and is consistent with the larger metallic radius of Fe (1.26 Å) compared with Ni (1.24 Å).[21] Increasing the iron content, further molybdenum metal and Fe_2N impurities were observed, although in contrast with the $(Ni,Cu)_2Mo_3N$ solid solutions the lattice parameter of the $(Ni,Fe)_2Mo_3N$ continued to increase, suggesting that there is no strong barrier to forming solid solutions in this more iron-rich region of the phase space. Based on the PXRD data the crystallite diameter of $(Ni,Fe)_2Mo_3N$ decreases with Fe content, and the BET surface areas increased with iron content (Table 2). The nitrogen content (combustion/CHN analysis) of the samples is approximately consistent with the calculated values. The TGA data during oxidation (ESI, Fig. S17 and Table S5†) showed the expected mass gains, with thermal stability decreasing with concentration of the second metal, similarly to the $(Ni,Cu)_2Mo_3N$ system. Electron microscopy (ESI, Fig. S18†) showed similar aggregates of particles to those of $(Ni,Cu)_2Mo_3N$, and EDX (ESI, Table S6†) showed expected compositions.

The ammonia synthesis rates of the $(Ni,Fe)_2Mo_3N$ catalysts increase with iron addition throughout the range of compositions where a single phase is formed, from 272 $\mu mol\ h^{-1}\ g^{-1}$ with Ni_2Mo_3N to 354 $\mu mol\ h^{-1}\ g^{-1}$ with $Ni_{1.1}Fe_{0.9}Mo_3N$ (Table 2). However, this increase appears to be linked to the increasing surface area with temperature, as the activities normalised by surface area have similar values.

Molybdenum nitrides have been reported as active catalysts for ammonia synthesis at 400 °C, and their catalytic performances are sometimes significantly improved by the addition of a second transition metal such as Ni, Co or Fe.[28,29] Kojima

Table 3 Surface areas, composition post-catalysis, ammonia synthesis rate and specific activity of metal oxide catalysts used directly in ammonia synthesis

Catalyst	Surface area (m^2 g^{-1})		Nitrogen content (wt %) post-catalysis[a]	Ammonia synthesis rate at 500 °C[b] (μmol g^{-1} h^{-1})	Specific activity at 500 °C[c] (μmol h^{-1} m^{-2})
	Pre-catalysis	Post-catalysis			
$Ni_2Mo_3O_x$	10	6	3.1	466(18)	78(3)
$Ni_{1.7}Cu_{0.3}Mo_3O_X$	6.6	4.8	3.3	368(9)	77(2)
$Ni_{1.2}Fe_{0.8}Mo_3O_X$	6.2	5.2	3.2	426(4)	82(1)

[a] Calculated values are 3.3–3.4%. [b] Conductivity profiles used to calculate these rates are shown in ESI (Fig. S32†). [c] Calculation based on the surface area of the nitride phase post-catalysis.

and Aika showed that cobalt molybdenum nitride promoted with Cs can synthesise ammonia at double the efficiency of commercial catalysts, with reported activities of 652 μmol g^{-1} h^{-1} and 986 μmol g^{-1} h^{-1}.[5,6,30–34] The high activity of the Co_3Mo_3N has been linked to the fact that CoMo alloy has an average nitrogen adsorption energy close to the optimal nitrogen binding energy for catalytic performance,[35,36] and to lattice nitrogen activity.[2,7,8,10,11,14,32,37] Activities for Ni_2Mo_3N and doped analogues are typically lower than those of Co_3Mo_3N-based catalysts despite the structural and electronic similarities between these two systems, and that may be linked at least partly to the lack of lattice nitrogen mobility exhibited by Ni_2Mo_3N.[11] Activities observed here are significantly higher than those observed in many other studies of this material and were seen to increase with iron doping, although our activities were measured at 500 °C due to a relatively low activity observed at 400 °C (ESI, Fig. S29†). Comparison of PXRD patterns collected before and after catalysis (ESI, Fig. S30 and S31†) shows no appreciable change to the structures throughout the series of samples. The nitrogen contents of the catalysts post-catalysis (combustion/CHN analysis, Tables 1 and 2) also remain consistent with the stoichiometric compositions. In addition to the linear conductivity changes observed in the catalysis, this suggests that the catalysts are stable under the reaction conditions used.

It has previously been noted that Ni_2Mo_3N can be synthesised from oxides at 700 °C using hydrogen–nitrogen mix, a key advantage compared with Co_3Mo_3N as it means the ammonia synthesis catalyst can be produced *in situ* under conditions typically used for catalyst activation, not requiring an ammonia firing step before use.[10,38] The citrate gel process led to a mixture (Fig. 6) of α-$NiMoO_4$ and MoO_3, which is consistent with the previously published observations of Alconchel *et al.*[22] Catalysis used the same conditions as the metal nitrides described above, with the activation step at 700 °C used to convert the oxides to nitrides and catalysis carried out at 500 °C, again resulting in a steady rate of ammonia production. Interestingly these materials exhibited significantly higher mass-normalised ammonia synthesis rates (Table 3). The surface areas were found to be higher than in the pre-formed nitrides both before and after catalysis (Table 3). Post-catalysis the PXRD patterns and compositions were very similar to those of the pre-formed nitrides (Fig. 6). We infer

from this that the transformation to the filled β-manganese type nitride phases proceeds smoothly under the catalyst activation conditions (700 °C under 75% H_2/25% N_2 yielding a higher surface areas that is advantageous in the catalytic process. Use of ammonia in the synthesis at this temperature yields a rocksalt-type impurity.[10,11] The activity has not scaled linearly with surface area, and these catalysts have lower area-normalised activities than the pre-formed nitrides (Tables 1–3), but nonetheless the increase supports the idea that increasing surface area could lead to higher overall activity levels in these materials.

Conclusions

Filled β-manganese type materials with composition Ni_2Mo_3N and with some Ni sites replaced by Cu or Fe were prepared by a citrate gel route. In both cases there was a limit to the amount of the second metal that could be substituted under these conditions, in the copper case that seemed to be due to a solubility limit of copper in the host phase. Iron doping increased the activity of the phase as a catalyst for ammonia synthesis at 500 °C and copper decreased that activity, but in both cases surface area, rather than any electronic differences, appear to be the main contributor to the observed change. The oxide intermediates could be converted to the nitride phases during the catalyst activation, avoiding the need to fire in ammonia. The *in situ* transformation of the oxides led to higher catalyst surface areas and hence to higher activity.

Conflicts of interest

There are no conflicts to declare.

Acknowledgements

References

1 Y. Nishibayashi, *Inorg. Chem.*, 2015, **54**, 9234–9247.

2 J. S. J. Hargreaves, *Coord. Chem. Rev.*, 2013, **257**, 2015–2031.

3 M. Nagai, *Appl. Catal., A*, 2007, **322**, 178–190.

4 E. Furimsky, *Appl. Catal., A*, 2003, **240**, 1–28.

5 R. Kojima and K. I. Aika, *Appl. Catal., A*, 2001, **218**, 121–128.

6 C. J. H. Jacobsen, *Chem. Commun.*, 2000, 1057–1058.

7 C. D. Zeinalipour-Yazdi, J. S. J. Hargreaves and C. R. A. Catlow, *J. Phys. Chem. C*, 2015, **119**, 28368–28376.

8 S. M. Hunter, D. H. Gregory, J. S. J. Hargreaves, M. Richard, D. Duprez and N. Bion, *ACS Catal.*, 2013, **3**, 1719–1725.

9 I. A. Amar, R. Lan, C. T. G. Petit and S. Tao, *Electrocatalysis*, 2015, **6**, 286–294.

10 N. Bion, F. Can, J. Cook, J. S. J. Hargreaves, A. L. Hector, W. Levason, A. R. McFarlane, M. Richard and K. Sardar, *Appl. Catal., A*, 2015, **504**, 44–50.

11 S. Al Sobhi, N. Bion, J. S. J. Hargreaves, A. L. Hector, S. Laassiri, W. Levason, A. W. Lodge, A. R. McFarlane and C. Ritter, *Mater. Res. Bull.*, 2019, **118**, 110519.

12 P. S. Herle, M. S. Hegde, K. Sooryanarayana, T. N. Guru Row and G. N. Subbanna, *Inorg. Chem.*, 1998, **37**, 4128–4130.

13 T. J. Prior and P. D. Battle, *J. Solid State Chem.*, 2003, **172**, 138–147.

14 J. S. J. Hargreaves and D. Mckay, *J. Mol. Catal. A: Chem.*, 2009, **305**, 125–129.

15 *PDF-2 (Powder Diffr. File), 2012 release, Int. Cent. Diffr. Data*, Swart. PA.

16 A. C. Larson and R. B. Von Dreele, *General Structure Analysis System (GSAS)*, Los Alamos National Laboratory Report LAUR 86-LAUR 748, 2000.

17 B. H. Toby, *J. Appl. Crystallogr.*, 2001, **34**, 210–213.

18 Inorg. Cryst. Struct. Database (ICSD, Fiz Karlsruhe) accessed via EPSRC-funded Natl. Chem. Database Serv. hosted by R. Soc. Chem.

19 S. Brunauer, P. H. Emmett and E. Teller, *J. Am. Chem. Soc.*, 1938, **60**, 309–319.

20 D. McKay, PhD thesis, University of Glasgow, 2008.

21 N. N. Greenwood and E. A. Earnshaw, *Chemistry of the Elements (2nd Ed.)*, Butterworth-Heinemann, 1997.

22 S. Alconchel, F. Sapiña, D. Beltrán and A. Beltrán, *J. Mater. Chem.*, 1999, **9**, 749–755.

23 A. Srifa, K. Okura, T. Okanishi, H. Muroyama, T. Matsui and K. Eguchi, *Catal. Sci. Technol.*, 2016, 7495–7504.

24 L. Volpe and M. Boudart, *J. Solid State Chem.*, 1985, **59**, 332–347.

25 J. G. Choi, J. R. Brenner, C. W. Colling, B. G. Demczyk, J. L. Dunning and L. T. Thompson, *Catal. Today*, 1992, **15**, 201–222.

26 D. W. Kim, D. K. Lee and S. K. Ihm, *Korean J. Chem. Eng.*, 2002, **19**, 587–592.

27 J. G. Choi, R. L. Curl and L. T. Thompson, *J. Catal.*, 1994, **146**, 218–227.

28 L. Volpe and M. Boudart, *J. Phys. Chem.*, 1986, **90**, 4874–4877.

29 S. T. Oyama, *Catal. Today*, 1992, **15**, 179–200.

30 D. Mckay, D. H. Gregory, J. S. J. Hargreaves, S. M. Hunter and X. Sun, *Chem. Commun.*, 2007, **7**, 3051–3053.

31 D. Mckay, J. S. J. Hargreaves, J. L. Rico, J. L. Rivera and X. L. Sun, *J. Solid State Chem.*, 2008, **181**, 325–333.

32 I. Alshibane, A. Daisley, J. S. J. Hargreaves, A. L. Hector, S. Laassiri, J. L. Rico and R. I. Smith, *ACS Sustainable Chem. Eng.*, 2017, **5**, 9214–9222.

33 R. Kojima and K. I. Aika, *Appl. Catal., A*, 2001, **219**, 141–147.

34 R. Kojima and K. Aika, *Appl. Catal., A*, 2001, **215**, 149–160.

35 C. J. H. Jacobsen, S. Dahl, B. G. S. Clausen, S. Bahn, A. Logadottir and J. K. Nørskov, *J. Am. Chem. Soc.*, 2001, **123**, 8404–8405.

36 A. Boisen, S. Dahl and C. J. H. Jacobsen, *J. Catal.*, 2002, **186**, 180–186.

37 A. Daisley and J. S. J. Hargreaves, *J. Energy Chem.*, 2019, **39**, 170–175.

38 J. O. Conway and T. J. Prior, *J. Alloys Compd.*, 2019, **774**, 69–74.